Towards Power FPGA: Architecture, Modeling and Control of Multiport Power Converters

Ping Wang, Minjie Chen
Department of Electrical Engineering
Andlinger Center for Energy and the Environment
Princeton University, Princeton, NJ 08540, USA
{pwang2,minjie}@princeton.edu

***Abstract*—Multiport power converters are needed in a wide range of applications including battery management systems, data center power delivery, and renewable energy systems. These systems comprise numerous distributed and modular power conversion cells with sophisticated and bidirectional power flow. This paper systematically investigates the architecture, modeling and control of multiport power converter with a large number of ports, and explores the theoretical foundation of an emerging "Power FPGA" concept - Flexible, Programmable, Granular and Adaptive power electronics - that will enable a wide range of exciting applications. We classified multiport power converters into two major categories, and developed a software tool based on Newton-Raphson method to rapidly identify the control strategy. We analyzed the applicability and limitations of this control framework, and simulated a 100-port energy converter with programmable power flow. A four-port programmable energy converter is built and tested to experimentally validate the proposed modeling and control strategy.**

***Index Terms*—multiport power converter, energy router, power flow calculation, Power FPGA**

I. Introduction

Power electronics are key building blocks of future energy systems. Developing flexible, programmable, granular and adaptive (FPGA) architectures will benefit a variety of emerging and high-impact applications, including EV chargers, battery management systems, data centers, and solar inverters. Future data centers, energy storage systems and solar farms comprise numerous modular power electronics cells configured as a sophisticated power processing network (Fig. 1): solar panels need maximum power point tracking; battery cells need voltage and state-of-charge (SOC) balancing; data centers need uninterruptable power supplies (UPS) and brick converters. These power electronics modules regulate the voltage, process power flow, and perform advanced power management functions. High performance power conversion architectures are needed to improve the efficiency and power density of these energy systems.

A conventional way to develop power conversion architecture for these systems is to create one or more dc buses with large capacitors as dc links, and connect each individual module to the dc link through a dc-dc converter. Each converter is controlled individually with classic control methods. As illustrated in Fig. 2(a), to deliver energy from one module to another, two or more "dc-ac-dc power conversion stages

978-1-5386-5541-2/18/$31.00 ©2018 IEEE

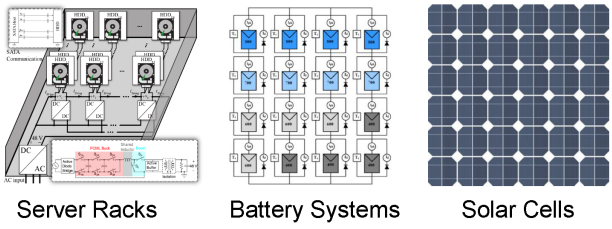

Fig. 1. Energy systems with numerous modular power converters.

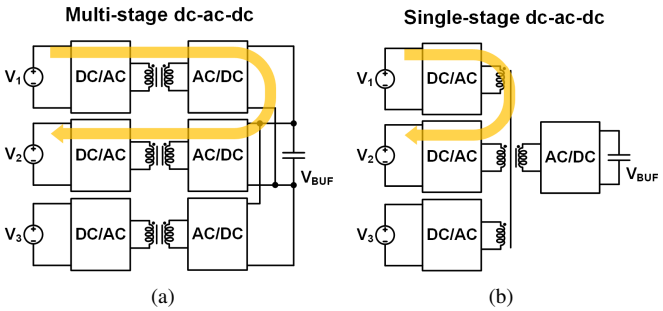

Fig. 2. Power flow in (a) a multiport converter with multiple "dc-ac-dc" stages; (b) a multiport converter with a single "dc-ac-dc" stage.

are usually needed. These "back-to-back" power conversion stages increases the component counts and reduces the energy efficiency. Methods to improve the performance of these multi-stage power conversion architectures exist, including the "differential power processing" concept [1], the "composite power conversion" architecture [2], and the "multiport energy router" concept [3]. The key principle is to reduce the power conversion stress and improve the energy efficiency and power density. Multiport power converters which can create a single "dc-ac-dc" path between any input and output port with programmable power flow (e.g., through a single-core multi-winding transformer), namely "Power FPGA", are rarely explored and are the main focus of this paper.

Fig. 2 compares a conventional multiport power conversion architecture with multiple "dc-ac-dc" stages, against a multiport architecture with a single "dc-ac-dc" stage between any arbitrary input-output ports. Instead of processing power with many individual dc-dc converters, single-stage architecture links multiple ports through a single magnetic-linkage with ac

coupling. Power flow is controlled by adjusting the voltage amplitude and phase shift of each port. A single stage architecture offers lower component count and higher efficiency, but the power flow control becomes more sophisticated. The control and modeling of multiport power converter coupled through a single magnetic have been previously explored [4]–[6]. [4] proposes a control method which operates the single-stage multiport architecture as a multi-active-bridge (MAB) and decouples the cross-regulation by linearizing the power flow equation with small signal model under the assumption that initial operating point is known. [5] explores the feasibility of using classic feedback control in a multiport energy router. [6] investigates the modeling and control of the MAB converters. The operation principles of these converters cannot be generalized to cover a large number of ports, and the applicability and limitations of these methods are not thoroughly explored.

This paper systematically investigates the architecture, modeling and control of multiport power converter with a large number of input and output ports. The operation of each port is programmable, allowing the multiport power converter to function as an energy processor. In addition, we studied the applicability and limitations of the proposed method and showed that the proposed method can be used to programme the power flow of a converter with 100 active ports. The theoretical foundation towards an exciting "Power FPGA" concept is explored - Flexible, Programmable, Granular and Adaptive power electronics - which will enable a wide range of new applications.

The followings of this paper are organized as follows. Section II develops a general circuit structure for multiport power converters. Section III discusses the two operation modes for multiport power converters, depending on the impedance of the passive network. A generalized modeling and control framework is developed in section IV. Section V discusses the convergence region and the maximum power rating of the multiport power converter. Finally, simulation and experiment results are presented in section VI and VII.

II. Architecture and Circuit Topology

Fig. 3 shows the architecture of a generalized multiport power converter, comprising n input and output ports (here $n = 6$). Operating all the dc-ac converters at the same frequency, the current and voltage in the power delivery network can be either sinusoidal or trapezoid depending on the impedance values of the passive network. By modulating the dc-ac converters, the energy processed at each port can be adjusted, and the power flow on each network branch can be precisely controlled.

Fig. 4 shows an example topology for the multiport power converter, where multiple active bridges are coupled through a single magnetic core. This topology offers galvanic isolation for each port and can link many ports with different voltage levels together. The active bridges can be full bridges or half bridges. While a half bridge implementation offers lower component count, a full bridge implementation offers flexible voltage regulation by phase shifting the two half bridge legs.

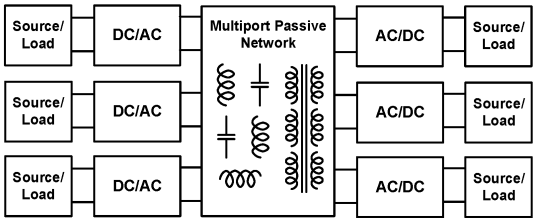

Fig. 3. Block diagram of multiport power converters comprising many dc/ac converters, and a single multiport passive network.

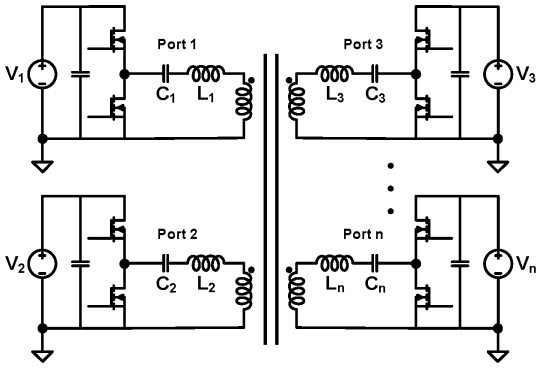

Fig. 4. Example topology of a multiport power converter with multiple half-bridges coupled together with a multi-winding transformer.

A transformer with an arbitrary number of windings can be modeled as a passive network comprising inductors, capacitors, resistors, and ideal transformers [7]. Fig. 5(a) demonstrates a Star model of the multi-winding transformer, in which all sources/loads are normalized to the primary side through ideal transformers. Each port is connected to the ground-connected magnetizing inductance L_m through a series LC network. The series capacitor of each branch can either function as a dc-blocking capacitor or a series-resonant capacitor depending on the values of the capacitor and the inductor of each branch. If the capacitor size is large enough to be considered as a dc-blocking capacitor, the current waveforms are trapezoidal; if the capacitor size is small enough, and the resonant frequency of the LC tank is close to the switching frequency, the LC network will function as a bandpass filter and the waveforms are sinusoidal. A Star model is interchangeable with a n-port Delta model or a n-port impedance matrix [8], as illustrated in Fig. 5(b).

III. Power Flow Modeling

The modeling and control of the power converter depend on the configuration of the passive network. The multiport power converter has the following two operation modes:

A. Trapezoidal Mode

If the series capacitance is large enough, the reactance of each branch at the switching frequency is dominated by the series-inductance:

$$\frac{X_L + X_C}{X_L} \approx 1. \tag{1}$$

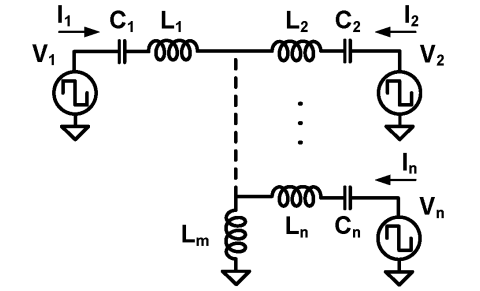

(a)

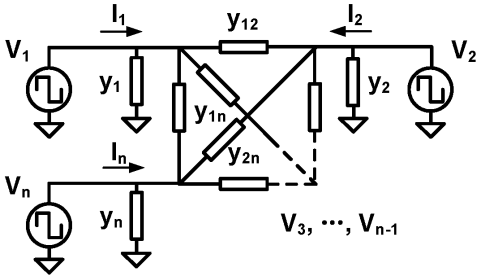

(b)

Fig. 5. (a) Star model and (b) Delta model of a multi-winding passive network. The Star model and Delta model are interchangeable through a $n \times n$ impedance matrix [8].

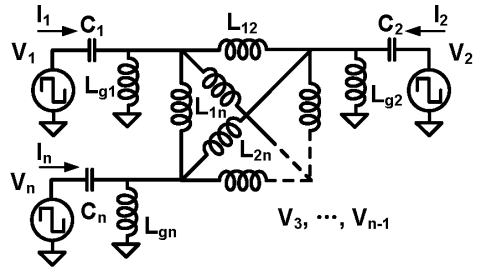

Fig. 6. A Delta model which is interchangable with the Star-type inductor network. The series capacitors are kept the same and the Star structure is converted to a Delta structure.

Each branch can be treated as an inductor connected in series with a dc-blocking capacitor, and the capacitance value has negligible impact on the branch reactance. Therefore, only the inductors are considered in the Star-to-Delta network conversion as shown in Fig. 6. The multiport power converter functions as a multi-active-bridge (MAB) converter [4], [9], [10], delivering power with trapezoidal current waveforms.

In a Delta model, the ground-connected inductor L_{gi} has no impact on the active power at each port - it only contributes reactive power. The inductance of L_{ij} between port i and port j can be calculated from the branch inductance of the Star model (L_1 to L_n in Fig. 5(a)) following Thevenin theorm [4]:

$$L_{ij} = \big(L_i + L_{THi}\big)\left[L_j\left(\frac{1}{L_m} + \sum_{k\neq i,j}^{n}\frac{1}{L_k}\right) + 1\right], \quad (2)$$

where the Thevenin-equivalent inductance seen by port i is:

$$L_{THi} = \left(\frac{1}{L_m} + \sum_{k\neq i}^{n}\frac{1}{L_k}\right)^{-1}. \quad (3)$$

Similar to a dual-active-bridge model, the active power carried by L_{ij} is a function of the voltage amplitude and phase difference between port i and port j [11]:

$$P_{ij} = \frac{1}{T}\int_T V_i I_{ij} dt = \frac{V_i V_j}{\omega L_{ij}}\phi_{ij}\left(1 - \frac{|\phi_{ij}|}{\pi}\right). \quad (4)$$

Here V_i is the voltage amplitude of the square wave voltage at port i. In fact, (4) is valid if and only if ϕ_{ij} is within $[-\pi, \pi]$. Phase difference that exceeds $[-\pi, \pi]$ should be converted back to this range. Define a function $\Phi(\phi)$ as:

$$\Phi(\phi_{ij}) = \phi_{ij} - 2k\pi, \phi_{ij} \in [2k\pi - \pi, 2k\pi + \pi]. \quad (5)$$

The active power flow from port i to port j is:

$$P_{ij} = \frac{V_i V_j}{\omega L_{ij}}\Phi(\phi_{ij})\left(1 - \frac{|\Phi(\phi_{ij})|}{\pi}\right). \quad (6)$$

The total injected power at port i is:

$$\begin{aligned} P_i &= \frac{1}{T}\int_T V_i I_i dt = \sum_{j\neq i}\frac{1}{T}\int_T V_i I_{ij} dt \\ &= \sum_{j\neq i}\frac{V_i V_j}{\omega L_{ij}}\Phi(\phi_{ij})\left(1 - \frac{|\Phi(\phi_{ij})|}{\pi}\right). \end{aligned} \quad (7)$$

B. Resonant Mode

If the resonant frequency of the series LC tank is close to the switching frequency, the branch reactance of each port is close to zero:

$$\frac{X_L + X_C}{X_L} \approx 0. \quad (8)$$

The series LC tank functions as a band-pass filter with low impedance at the resonant frequency. It eliminates the higher order current harmonics so that the current in the passive network is close to sinusoidal. As a result, the multiport power converter can be considered as an ac power delivery network driven by n sinusoidal voltage sources, since only the fundamental component of the square wave voltage can deliver real power. The impedance matrix of the passive network in Fig. 5(a) is:

$$Z = \begin{bmatrix} Z_{b1} + Z_m & Z_m & \dots & Z_m \\ Z_m & Z_{b2} + Z_m & \dots & Z_m \\ \vdots & \vdots & \ddots & \vdots \\ Z_m & Z_m & \dots & Z_{bn} + Z_m \end{bmatrix}. \quad (9)$$

Z_{bi} is the branch impedance connected to port i, and Z_m is impedance of the magnetizing inductance.

$$Z_{bi} = j\left(\omega L_i - \frac{1}{\omega C_i}\right), \quad Z_m = j\omega L_m. \quad (10)$$

The admittance of the interchangeable Delta model of the Star model is the inverse of the impedance matrix Eq. (9):

$$Y = Z^{-1} = \begin{bmatrix} Y_{11} & \dots & Y_{1n} \\ \vdots & \ddots & \vdots \\ Y_{n1} & \dots & Y_{nn} \end{bmatrix}, \tag{11}$$

$$Y_{ij} = G_{ij} + B_{ij} = \begin{cases} y_i + \sum_{k \neq i} y_{ik} & if\ i = j \\ -\, y_{ij} & if\ i \neq j \end{cases} \tag{12}$$

Based on theories in power systems analysis [12], the active power injected into each port is:

$$P_i = \frac{8}{\pi^2} \sum_{k=1}^{n} V_i V_k \left(G_{ik} \cos(\phi_{ik}) + B_{ik} \sin(\phi_{ik}) \right). \tag{13}$$

Here V_i and V_k are the amplitudes of the square wave voltage at port i and port k.

IV. A Generalized Control Framework

Four variables are controllable at each port of the multiport power converter, (P_i, Q_i) and (V_i, ϕ_i). P_i and Q_i are the active and reactive power injected into the i^{th} port from an external source or load. V_i and Φ_i are the amplitude and phase of the square wave voltage at each port. In power electronics designs, the reactive power at each port is usually absorbed by a large dc-filtering capacitor and is usually neglected. Depending on the design goals, one can control the voltage amplitude and the phase shift to modulate the injected power, or control the injected power and the phase shift to modulate the voltage of each port. When designing the control framework, the n ports can be grouped into two major categories:

- PV port: P_i and V_i are specified, and ϕ_i is unknown. In multiport power converters, sources and loads that require specific voltage amplitudes or active power injection can be modeled as PV ports.
- Vϕ port: the reference port for the power flow calculation. V_i is selected as the nominal voltage, ϕ_i is considered as zero, P_i is free-wheeling and is determined by the system needs. At least one Vϕ port is needed in a system to meet the energy conservation requirements. Usually, a port that is connected to an energy storage device can be selected as a Vϕ port.

In a multiport power converter, a majority of ports are PV ports. A port that is connected to an energy storage element is usually selected as the $V\phi$ port. The $V\phi$ port functions as an energy buffer to balance the input and output power of the system. As a result, a multiport power converter with n ports usually has $n-1$ PV ports and one $V\phi$ port. The phases of all n ports need to be precisely controlled to control the power flow in the multiport passive network. The target of this control framework is the active powers of the $n-1$ PV ports; the input variables are the phases of the voltage of all of the $n-1$ ports (the phase of the $V\phi$ port is zero). The key challenge of this control framework is to solve $n-1$ unknown variables with $n-1$ nonlinear power flow equations:

$$\begin{bmatrix} P_1 \\ P_2 \\ \vdots \\ P_{n-1} \end{bmatrix} = f : R^{n-1} \rightarrow R^{n-1} \begin{bmatrix} \phi_1 \\ \phi_2 \\ \vdots \\ \phi_{n-1} \end{bmatrix}. \tag{14}$$

We adopted the Newton-Raphson method in power system analysis [12] to solve these nonlinear equations. Newton-Raphson method linearizes non-linear equations and use iterations to approach desired solutions. It converges fast and requires low computation power (enabling a microcontroller or FPGA implementation), but is sensitive to the initial anticipated solution. A software tool is developed open-sourced in Github [1]. Other methods such as Gauss-Seidel Iteration and Fast Decoupling Methods [12] may be applicable to specific cases. Sophisticated power flow calculation tools such as Matpower [13] can also be used at the cost of more computation requirements. In this work, a Newton-Raphson solver customized for power flow analysis in both trapezoidal and resonant modes has been developed and open sourced. The solver takes in the following inputs: 1) network information: including the branch inductance, magnetizing inductance, branch capacitance and branch resistance; 2) targeted active power and voltage amplitude of PV ports; 3) voltage amplitude of the reference port; 4) initial anticipated solutions for the phases of each port. The iteration step for the solver is:

$$\begin{bmatrix} \Delta\phi_1 \\ \Delta\phi_2 \\ \vdots \\ \Delta\phi_{n-1} \end{bmatrix} = \begin{bmatrix} \frac{\partial f_1}{\partial \phi_1} & \dots & \frac{\partial f_1}{\partial \phi_{n-1}} \\ \vdots & \ddots & \vdots \\ \frac{\partial f_{n-1}}{\partial \phi_1} & \dots & \frac{\partial f_{n-1}}{\partial \phi_{n-1}} \end{bmatrix}^{-1} \begin{bmatrix} \Delta P_1 \\ \Delta P_2 \\ \vdots \\ \Delta P_{n-1} \end{bmatrix}, \tag{15}$$

$$\boldsymbol{\phi}_k = \boldsymbol{\phi}_{k-1} - \Delta\boldsymbol{\phi}. \tag{16}$$

The Jacobian matrix for trapezoidal mode is:

$$\frac{\partial f_i}{\partial \phi_j} = \begin{cases} \frac{V_i V_j}{\omega L_{ij}} \left(\frac{2|\Phi(\phi_{ij})|}{\pi} - 1 \right) & j \neq i \\ \sum_{k \neq i} \frac{V_i V_k}{\omega L_{ik}} \left(1 - \frac{2|\Phi(\phi_{ik})|}{\pi} \right) & j = i \end{cases} \tag{17}$$

The Jacobian matrix for resonant mode is:

$$\frac{\partial f_i}{\partial \phi_j} = \begin{cases} \frac{8}{\pi^2} V_i V_j \left[G_{ij} \sin(\phi_{ij}) - B_{ij} \cos(\phi_{ij}) \right] & j \neq i \\ \sum_{k \neq i} \frac{8}{\pi^2} V_i V_k \left[B_{ik} \cos(\phi_{ik}) - G_{ik} \sin(\phi_{ik}) \right] & j = i \end{cases} \tag{18}$$

With appropriate selection of the initial operating point, the phases of all ports can usually be found within a few iteration steps. These phases will be utilized to control the ac-dc converters at each port. If full bridges are implemented as the dc/ac converters in Fig. 4, or the source voltage is variable within a range, more feasible solutions can be found for the the nonlinear power flow equations. These ports can be defined as P ports with only active power in control. Assuming there are n ports in total, the first m ports are P ports, and the last port

[1] https://github.com/PingWang3741/Multiport-Power-Converter.git

is a reference port, the rest of them are P ports. The iteration step of the solver is:

$$\begin{bmatrix} \Delta V_1 \\ \cdots \\ \Delta V_m \\ \Delta\phi_1 \\ \vdots \\ \Delta\phi_{n-1} \end{bmatrix} = \begin{bmatrix} \frac{\partial f_1}{\partial V_1} & \cdots & \frac{\partial f_1}{\partial V_m} & \frac{\partial f_1}{\partial \phi_1} & \cdots & \frac{\partial f_1}{\partial \phi_{n-1}} \\ \vdots & \ddots & \vdots & \vdots & \ddots & \vdots \\ \frac{\partial f_{n-1}}{\partial V_1} & \cdots & \frac{\partial f_{n-1}}{\partial V_m} & \frac{\partial f_{n-1}}{\partial \phi_1} & \cdots & \frac{\partial f_{n-1}}{\partial \phi_{n-1}} \end{bmatrix}^{-1} \begin{bmatrix} \Delta P_1 \\ \Delta P_2 \\ \vdots \\ \Delta P_{n-1} \end{bmatrix}, \tag{19}$$

$$\boldsymbol{V}_k = \boldsymbol{V}_{k-1} - \Delta \boldsymbol{V}, \quad \boldsymbol{\phi}_k = \boldsymbol{\phi}_{k-1} - \Delta\boldsymbol{\phi}. \tag{20}$$

There are $n-1+m$ unknown variables and $n-1$ nonlinear equations. The Jacobian matrix is not a square matrix. The Moore-Penrose pseudoinverse of the Jacobian matrix can be utilized to calculate the iteration step size. When V_i of the i^{th} P port reaches its maximal value, this P port will change back to PV port in the next iteration.

V. Power Rating and Convergence Discussion

It is known that the convergence of the Newton-Raphson method is very sensitive to the initial anticipated solution. The Newton-Raphson method will not converge if there is no feasible solution. As a result, its critical to determine if the targeted solution is even feasible before the iteration starts. Given a general n-port system with arbitrary branch capacitance and inductance as shown in Fig. 5(a), the passive network can be transformed either to a Delta network as shown in Fig. 5(a) or an impedance Delta network as shown in Fig.5(b). If the multiport converter works in trapezoidal mode, the maximal power injected into port i and the maximum power extracted from port i are:

$$P_{i\_\max} = \frac{\pi}{4} \sum_{k \neq i} \frac{V_i V_k}{\omega L_{ik}}, \tag{21}$$

$$P_{i\_\min} = -\frac{\pi}{4} \sum_{k \neq i} \frac{V_i V_k}{\omega L_{ik}}. \tag{22}$$

If the multiport power converter works resonant mode, the maximal and minimal feasible power at port i are:

$$P_{i\_\max} = \max(a|V_i|^2 + b|V_i|), \tag{23}$$

$$P_{i\_\min} = \min(a|V_i|^2 - b|V_i|), \tag{24}$$

where

$$\begin{aligned} b &= \frac{8}{\pi^2} \sum_{k \neq i} V_{k\_\max} \sqrt{G_{ik}^2 + B_{ik}^2}, \\ a &= -\frac{8}{\pi^2} \sum_{k \neq i} G_{ik}. \end{aligned} \tag{25}$$

$V_{\max}$ is the maximal amplitude of the square wave voltage at port i. Equation (23) is the maximal value of a quadratic function, which can be rewritten as a piecewise function:

$$P_{\max} = \begin{cases} \frac{8}{\pi^2} \sum_{k \neq i} \left(V_{k\_\max} \sqrt{G_{ik}^2 + B_{ik}^2} - V_{i\_\max} G_{ik} \right) V_{i\_\max} & if\ a \geq 0 \\ \frac{8}{\pi^2} \frac{\left(\sum_{k \neq i} V_{k\_\max} \sqrt{G_{ik}^2 + B_{ik}^2} \right)^2}{4 \sum_{k \neq i} G_{ik}} & if\ a < 0\ \ \&\ \ -\frac{b}{2a} \leq V_{i\_\max} \\ \frac{8}{\pi^2} \sum_{k \neq i} \left(V_{k\_\max} \sqrt{G_{ik}^2 + B_{ik}^2} - V_{i\_\max} G_{ik} \right) V_{i\_\max} & if\ a < 0\ \ \&\ \ -\frac{b}{2a} > V_{i\_\max} \end{cases} \tag{26}$$

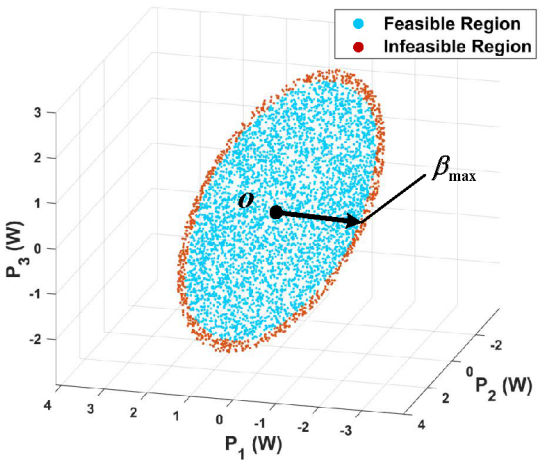

Fig. 7. Feasible power range of a three-port converter.

Similarly, Equation (24) can be rewritten as:

$$P_{\min} = \begin{cases} -\frac{8}{\pi^2} \sum_{k \neq i} \left(V_{k\_\max} \sqrt{G_{ik}^2 + B_{ik}^2} + V_{i\_\max} G_{ik} \right) V_{i\_\max} & if\ a < 0 \\ \frac{8}{\pi^2} \frac{\left(\sum_{k \neq i} V_{k\_\max} \sqrt{G_{ik}^2 + B_{ik}^2} \right)^2}{4 \sum_{k \neq i} G_{ik}} & if\ a \geq 0\ \ \&\ \ \frac{b}{2a} \leq V_{i\_\max} \\ -\frac{8}{\pi^2} \sum_{k \neq i} \left(V_{k\_\max} \sqrt{G_{ik}^2 + B_{ik}^2} + V_{i\_\max} G_{ik} \right) V_{i\_\max} & if\ a \geq 0\ \ \&\ \ \frac{b}{2a} > V_{i\_\max} \end{cases} \tag{27}$$

No all ports input the maximum rated power. In applications such as differential power processing of series-stacked data center sever [1], all ports are identical with symmetric passive network. We use the sum of power squares (SPS) to describe the feasible power range of multiple ports. The SPS defines an active power region that is a conservative subset of the complete feasible power region. A very conservative definition of the feasible power region is:

$$\sum_{i=1}^{n} P_i^2 \leq \beta_{max}, \tag{28}$$

where β_{max} is a pre-determined bound that guarantees a feasible solution if Eq. (28) holds true.Assuming the multiport converter works in the resonant mode and all branch susceptances in the Delta model are identical. Here we use a three-port converter as an example to demonstrate the effectiveness of using SPS as a convergence bound. We swept the voltage amplitudes and phases of the three ports and record the feasible power that can be achieved at each port, and plot the results in Fig. 7. The blue points are the feasible power region, and the red points are infeasible power region. The inner circle of the blue-point area is a conservative bound for the feasible power range as described by Eq. (28). This area is smaller than the real feasible power range, but it is close enough.

The convergence region of the Newton-Raphson method is also determined by the initial anticipated solutions. Using the developed Newton-Raphson solver, a three-port converter is tested, where two ports are PV port, and the other one is Vϕ port. We selected a target power solution and swept the initial phase of the two ports from $-\pi$ to π, and record if the solver converge to a feasible solution. It is found that

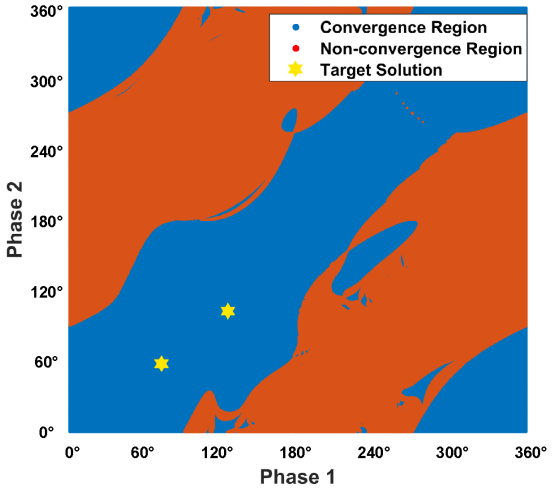

Fig. 8. Fractal convergence region of the Newton-Raphson solver. The solver is more likely to converge if the initial anticipated points are close to the final solution. Empirically, for a symmetric multiport network, starting from the origin is always a good strategy.

two feasible solution exist, and the converging area for the initial phases have fractal boundary. It also indicates that initial solutions that are close to the feasible solution converges better. With a look-up table that store a certain number of known solutions, the solver can always start from a initial point near the final solution to ensure the convergence of the algorithm. We found that for a multiport system with identical impedances on all branches, using zero phase-shift and uniform voltage amplitude as the initial solution almost always lead to a converging result, if the targeted power solution is within a feasible region.

Fig. 8 shows the results. The convergent region has fractal boundary. Initial solutions that are close to the final solution are more likely to converge. Utilizing this feature, we can build up a look-up table to store a certain number of samples (injected power of each port and its corresponding phases). For each calculation, the solver will start from a initial point near the final solution to ensure the convergence.

VI. Simulation Results

A. Four-Port Simulation

A four-port converter with the topology in Fig. 4 is simulated to verify the effectiveness of the proposed approach. The leakage inductance of the windings are combined into the series resonant inductance. The capacitance values are adjusted to test the converter in trapezoidal mode and resonant mode. Table I listed the component values of the four-port converter.

In an example test case, we tried to control the injected power of the four ports to be (25W, 5W, -10W, -20W). The calculated phase for the four ports are (25.9°, 4.65°, -10.2°, -20.4°) and (3.86°, 0.771°, -1.54°, -3.09°) in trapezoidal mode and resonant mode respectively. The simulated voltage and current waveforms of the four ports are shown in Fig. 9. The current in the resonant options has lower THD as predicted.

TABLE I
Simulation Parameters

Parameter		Value
Source Voltage ($V_1 \sim V_4$)		30 V
Branch Inductance ($L_1 \sim L_4$)		1 μH
Magnetic Inductance (L_m)		10 μH
Branch Capacitance	Trapezoidal	10 μF
($C_1 \sim C_4$)	Resonant	0.12 μF
Switching Frequency (f_{sw})		500 kHz

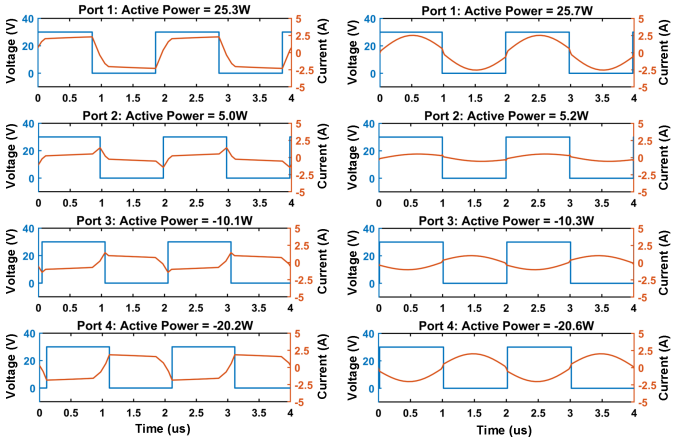

(a) (b)

Fig. 9. Input voltage and current waveforms of (a) trapezoidal mode operation and (b) resonant mode operation.

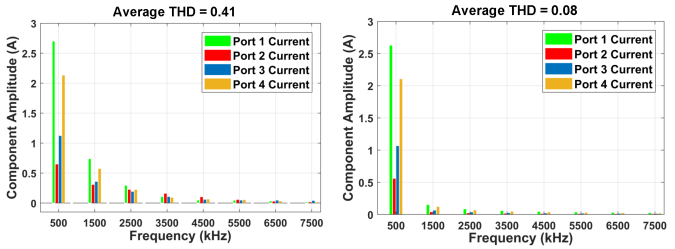

(a) (b)

Fig. 10. Harmonic analysis of (a) trapezoidal mode operation and (b) resonant mode operation.

The maximal error ratio between the targeted power and simulated power at each port for both cases is 4%.

For a specific multiport converter design, it is critical to know which mode is more accurate for controlling the power flow. A high impedance ratio Eq. (1) indicates that the multiport converter operates more like a multi-active-bridge converter, and a low impedance ratio indicates that the multiport converter operates more like a resonant converter. The power flow equations derived for MAB converter works well if the impedance ratio is higher than 0.8, but its accuracy drops rapidly if the impedance ratio is lower than 0.8. As shown in Fig. 11, the power flow equations derived for resonant operation maintains high accuracy across a wide impedance ratio range. As a result, it is generally valid to assume multiport power converters are operating in resonant mode to perform the power flow analysis while maintaining reasonable model accuracy. The simulation results well match the theory derived in section III.

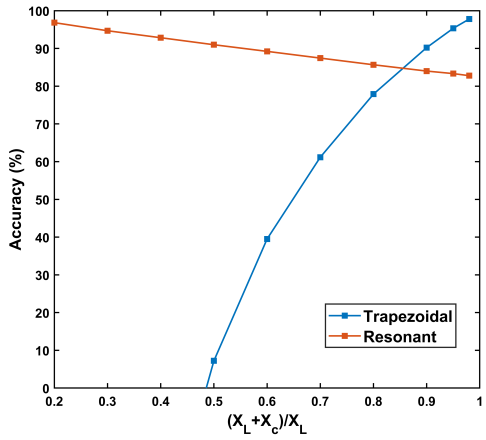

Fig. 11. Accuracy of two models. The trapezoidal model is more accurate in predicting the power flow in multi-active-bridge operation, and the resonant model is more accurate in predicting the power flow in resonant operation.

TABLE II
EXPERIMENT PARAMETERS

Parameter		Value
Branch Inductance ($L_1 \sim L_4$)		1.1μH
Equivalent Magnetic Inductance (L_m)		9.74 μH
Branch Capacitance	Trapezoidal	10 μF
($C_1 \sim C_4$)	Resonant	0.156 μF

B. One hundred port simulation

To verify the effectiveness of the proposed approach for very sophisticated energy systems, a 100-port simulation platform is built in PLECS (Fig. 12). The switching frequency, the branch LC values and the magnetic inductance are kept the same as the four-port simulation. The targeted power and the simulated power of 100 ports are listed and compared in Fig. 13. Simulated results match precisely with the targeted powers, and the maximal error of controlling power of the 100 port is about 1%. The simulation layout the theoretical foundations of the Power FPGA concept - with precisely controlled impedance of the passive network (e.g., through PCB embedded planar magnetics [7]) - the power flow among a large number of power ports can modulated and reprogrammed.

VII. EXPERIMENT RESULTS

Using a Star equivalent model of the transformer, a four-port power converter with the same port voltages and switching frequency as those in simulation is built to experimentally verify the proposed control framework. The branch element values and magnetic inductance is shown in Table II, and Fig. 14 shows the experiment setup. Both trapezoidal mode and resonant model have been implemented on the experiment platform, and the corresponding voltage and current waveforms are shown in Fig. 15.

The measured results of three example cases are listed in Table III. The experimental results match closely with the targets, and the mismatch mainly comes from switching losses, system parasitics and DSP control precision that are not captured in the model. With a feedback system that compensates the parasitics and non-linear effects [4], the prototype can precisely route the electric power among multiple ports.

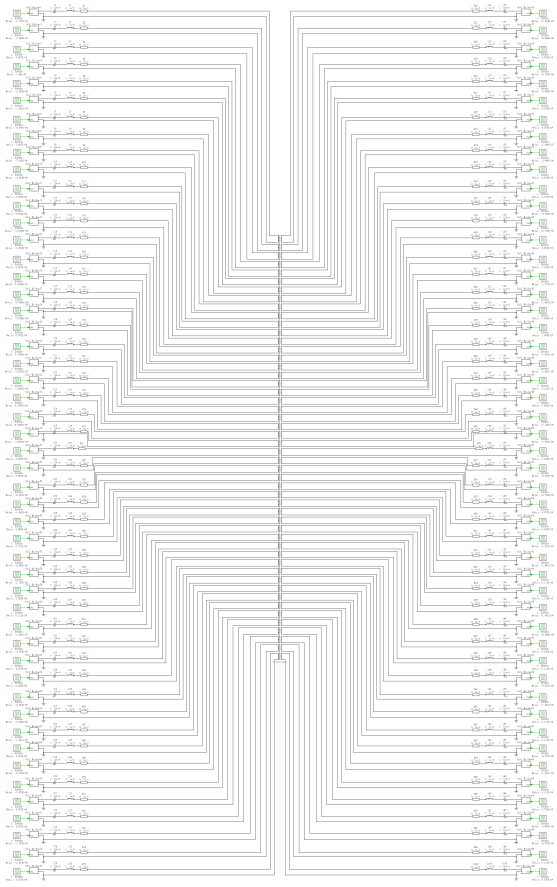

Fig. 12. A "Power FPGA" simulation platform with 100-ports.

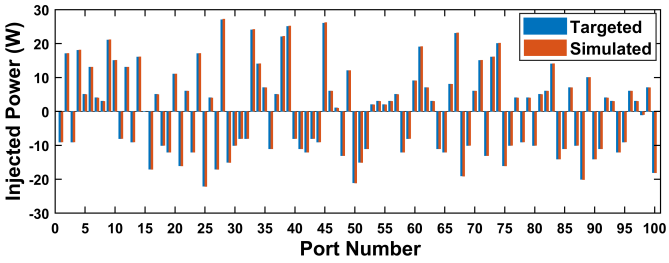

Fig. 13. Targeted and simulated real power injection at the 100 ports. The target power at all ports are programmable.

VIII. CONCLUSION

This paper develops a systematic modeling and control framework for multiport power converters with a very large number of input-output ports. We classify the multiport power converter into trapezoidal mode and resonant mode according to its passive network values, and develop two different power flow models to capture the two operation modes. A customized Newton-Raphson solver is designed to identify the cross-coupled control variables in the nonlinear power

TABLE III
EXPERIMENTAL VERIFICATION RESULTS.

Power(W)	Case I: Port-3 in; Port-1 out			Case II: Port-2, Port-3 in; Port-1 out			Case III: Port-2, Port-3, Port-4 in; Port-1 out		
	Targeted	Trapezoidal	Resonant	Targeted	Trapezoidal	Resonant	Targeted	Trapezoidal	Resonant
Port 1	-30.00	-27.25	-27.90	-30.00	-27.67	-27.40	-30.00	-27.83	-27.23
Port 2	0.00	0.90	0.30	10.00	10.80	9.30	5.00	5.10	4.80
Port 3	30.00	32.40	30.90	20.00	21.30	20.40	10.00	11.40	9.90
Port 4	0.00	0.60	0.90	0.00	0.60	0.90	15.00	15.60	15.3

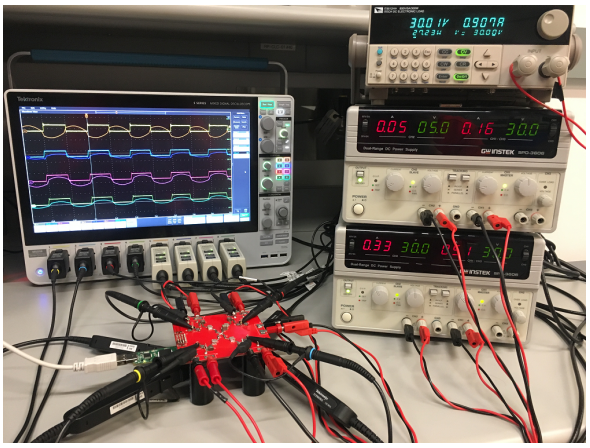

Fig. 14. Experiment setup of a four-port energy processing system.

flow equations. The proposed analytical models and theoretical analysis is verified by a four-port simulation platform, an 100-port simulation platform, and a four-port experimental platform. As a new development of the "Power FPGA" concept towards Flexible, Programmable, Granular and Adaptive power electronics, the proposed method will open exciting opportunities in designing high frequency power converters in a wide range of emerging applications.

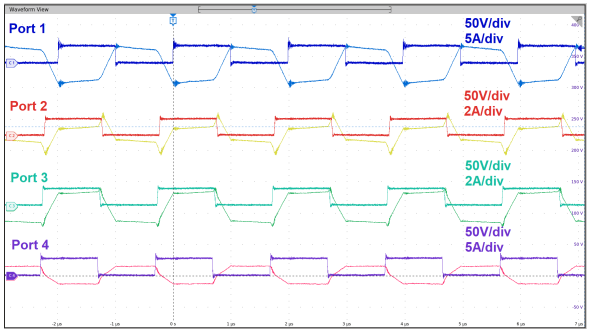

(a)

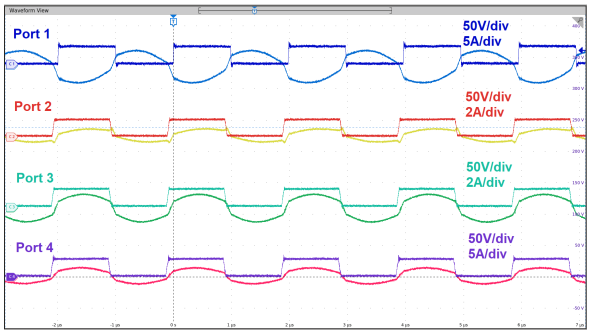

(b)

Fig. 15. Measured waveforms for experimental case III: (a) trapezoidal mode operation and (b) resonant mode operation.

REFERENCES

[1] E. Candan, P. S. Shenoy and R. C. N. Pilawa-Podgurski, "A Series-Stacked Power Delivery Architecture With Isolated Differential Power Conversion for Data Centers," *IEEE Transactions on Power Electronics*, vol. 31, no. 5, pp. 3690-3703, May 2016.

[2] H. Chen, H. Kim, R. Erickson and D. Maksimovic, "Electrified Automotive Powertrain Architecture Using Composite DC-DC Converters," *IEEE Transactions on Power Electronics*, vol. 32, no. 1, pp. 98-116, Jan. 2017.

[3] N. Bilakanti, L. Zheng, P. Kandula, K. Kandasamy and D. Divan, "Single Stage Soft-Switching Tri-Port Converter for Integrating Renewable Source and Storage with Grid through Galvanic Isolation," *European Conference on Power Electronics and Applications (EPE'17 ECCE Europe)*, Warsaw, 2017, pp. 1-10.

[4] S. Falcones, R. Ayyanar, and X. Mao, "A DCDC Multiport-Converter Based Solid-State Transformer Integrating Distributed Generation and Storage," *IEEE Transactions on Power Electronics*, 2013. 28(5): p. 2192-2203.

[5] X. Liu, Z. Zheng, K. Wang and Y. Li, "An energy router based on multi-winding high-frequency transformer," *2016 IEEE Applied Power Electronics Conference and Exposition (APEC)*, Long Beach, CA, 2016, pp. 3317-3321.

[6] P. Zumel, C. Fernandez, A. Lazaro, M. Sanz and A. Barrado, "Overall analysis of a modular multi active bridge converter," *2014 IEEE 15th Workshop on Control and Modeling for Power Electronics (COMPEL)*, Santander, 2014, pp. 1-9.

[7] M. Chen, M. Araghchini, K. K. Afridi, J. H. Lang, C. R. Sullivan and D. J. Perreault, "A Systematic Approach to Modeling Impedances and Current Distribution in Planar Magnetics," *IEEE Transactions on Power Electronics*, vol. 31, no. 1, pp. 560-580, Jan. 2016.

[8] D. Maksimovic, R. W. Erickson and C. Griesbach, "Modeling of Cross-Regulation in Converters Containing Coupled Inductors," *IEEE Transactions on Power Electronics*, vol. 15, no. 4, pp. 607-615, Jul 2000.

[9] H. Tao, A. Kotsopoulos, J. L. Duarte and M. A. M. Hendrix, "Family of Multiport Bidirectional DC-DC Converters," *IEE Proceedings - Electric Power Applications*, vol. 153, no. 3, pp. 451-458, 1 May 2006.

[10] G. Buticchi, L. F. Costa, D. Barater, M. Liserre and E. Dominguez, "A Quadruple Active Bridge Converter for the Storage Integration on the More Electric Aircraft," *IEEE Transactions on Power Electronics*, in press.

[11] R. W. A. A. De Doncker, D. M. Divan and M. H. Kheraluwala, "A Three-Phase Soft-Switched High-Power-Density DC/DC Converter for High-Power Applications," *IEEE Transactions on Industry Applications*, vol. 27, no. 1, pp. 63-73, Jan/Feb 1991.

[12] J. D. Glover, M. S. Sarma, and T. J. Overbye, *Power System Analysis and Design*, 4th ed. Toronto, ON, Canada: Thomson, 2008.

[13] R. D. Zimmerman, C. E. Murillo-Sanchez and R. J. Thomas, "MATPOWER: Steady-State Operations, Planning, and Analysis Tools for Power Systems Research and Education," *IEEE Transactions on Power Systems*, vol. 26, no. 1, pp. 12-19, Feb. 2011.